ELSEVIER

International Journal of Heat and Fluid Flow 22 (2001) 287–292

International Journal of HEAT AND FLUID FLOW

www.elsevier.com/locate/ijhff

Interactions of longitudinal vortices generated by twin inclined jets and enhancement of impingement heat transfer

Kazuyoshi Nakabe [a,*], Elzbieta Fornalik [b], Jens F. Eschenbacher [a], Yu Yamamoto [a], Tomoyasu Ohta [a], Kenjiro Suzuki [a]

[a] *Department of Mechanical Engineering, Kyoto University, Kyoto 606-8501, Japan*
[b] *University of Mining and Metallurgy, Al. Mickiewicza 30, 30-059 Krakow, Poland*

Abstract

The present study was provided to examine the interaction between two inclined impinging jets in in-line and staggered arrangements with crossflow. The experimental investigations on impingement heat transfer characteristics and flow structures were made using thermochromic liquid crystal, fluorescence dyes and particle image velocimetry, PIV, techniques. Color patterns of the liquid crystal images taken with a CCD video camera were transformed into target wall temperature distributions and then into Nusselt number distributions by means of neural network algorithm. The flow patterns were visualized by using fluorescent dye injected into the jets and illuminated by a planer CW laser light. The cross-sectional images of a planer pulse laser light scattered by fine tracer particles were estimated with the PIV system and presented as the velocity distributions. It was observed that the geometrical arrangement of the inclined jets had an influence on the interaction between the two jet flows, on the vortical structures generated in the downstream of the jets, and eventually on the enhanced regions of jet impingement heat transfer. The large-scale four longitudinal vortices were generated in the case of staggered arrangement of the two inclined jets, while in the case of in-line arrangement only three major vortices were observed.

Keywords: Jet impingement heat transfer; Crossflow; Twin jet interaction; Heat transfer coefficient; Longitudinal vortex; Flow visualization; PIV system

1. Introduction

Jet impingement is used in the wide range of industrial applications such as the drying process of papers and films, the tempering process of glass, the cooling process of gas turbines and electronic components, etc. Impinging jets have the advantages of effective removal of locally concentrated heat flux and easy adjustment to the locations where the jets are necessary for the drying and/or cooling. The jets are generally discharged through arrays of circular holes arranged in in-line or staggered fashion in order to prevent heat transfer rates from rapidly decreasing outside the locally enhanced region of a single impinging jet. Such multiple jet impingement, however, deteriorates heat transfer characteristics of downstream-positioned jets because of the crossflow produced by the confluence of upstream-positioned jets. Thus, many researchers including Metzger and Korstad (1972), Bouchez and Goldstein (1975), Sparrow (1975), Saad et al. (1980), Goldstein and Behbahani (1982) and Huang et al. (1996) have studied various aspects of the jet impingement heat transfer under the influence of crossflow. This problem is also in the field of interests of the authors who paid attention to a spanwisely oblique jet discharging into a duct flow and impinging onto a heat transfer target wall of the duct. Previous investigations of this jet show a larger enhanced area of impingement heat transfer in comparison with the case of a vertical jet (Nakabe et al., 1998a,b,c). The experimental results show also an interesting feature that the Nusselt number distribution becomes a plateau-like pattern, which means that the enhanced region of heat transfer expands more. But the value of maximum Nusselt number itself becomes lower because of the relatively longer impingement distance due to the oblique angle, which could be recognized as a disadvantage in some sense. The Nusselt number distribution depends on crossflow Reynolds number, *Re*, and also on the velocity ratio of the jet to the crossflow, VR. As the velocity ratio VR was increased, the heat transfer enhancement area was extended more widely, and the maximum heat transfer coefficient rose its value because of relatively smaller influence of the crossflow. The flow visualization demonstrated the generation of a pair of large-scale counter-rotating longitudinal vortices by this inclined impinging jet, and also the relation between the vortices' tracks and heat transfer enhancement region.

* Corresponding author. Tel.: +81-75-753-5251; fax: +81-75-753-5251.
E-mail address: nakabe@mech.kyoto-u.ac.jp (K. Nakabe).

0142-727X/01/$ - see front matter
PII: S0142-727X(01)00090-X

Notation

d	jet nozzle diameter
Nu	Nusselt number
Re	crossflow Reynolds number
VR	velocity ratio of jet to crossflow
x, y, z	streamwise, vertical and spanwise coordinate

Modern, high performance gas turbine engines operate at high turbine inlet temperature as much as possible to achieve the better performance. The temperature of turbine components should have the upper limit for the acceptable component life. Gas turbine, therefore, requires internal cooling of many components exposed to hot burnt gas flow (Son et al., 1996). The most important requirement is to obtain uniform heat flux distributions, which could be realized by multiple impinging jets. The new configuration of the jet nozzles, however, generates a problem, related to the interaction between the jets and also to the influence of the crossflow produced by the confluence of upstream multiple jets on heat transfer, as mentioned above. In the present study following the authors' previous experiment (Fornalik et al., 1999), the flow patterns and heat transfer distributions of two kinds of geometrical arrangements of twin inclined jets were visualized experimentally. The experimental conditions were the same as in the case of the single inclined jet previously investigated.

2. Experimental apparatus and methods

Fig. 1 shows the test section of a rectangular duct with two inclined impinging jets issuing into a fully developed turbulent crossflow. The height and width of the duct were 21 and 432 mm, respectively. The water was circulated in a closed circuit from a constant head tank, which was delivered to the main flow and jets and then returned to the head tank through a centrifugal pump. The nozzles were mounted flush with the bottom wall of the test section, and the jets through the nozzles impinge onto the upper target wall. Two geometrical configurations of the jet nozzles were introduced to the present experimental study. In Fig. 1(a), the two oblique jets are situated in in-line arrangement with a streamwise distance of 10 nozzle-diameters. The diameter of each nozzle was $d = 6$ mm. The skew angles measured relatively to the crossflow direction were set to be $-90°$ for the upstream-side jet, Jet 1, and $+90°$ for the downstream-side one, Jet 2, while the pitch angle measured up from the nozzle-installed wall was fixed at 45° for both jets.

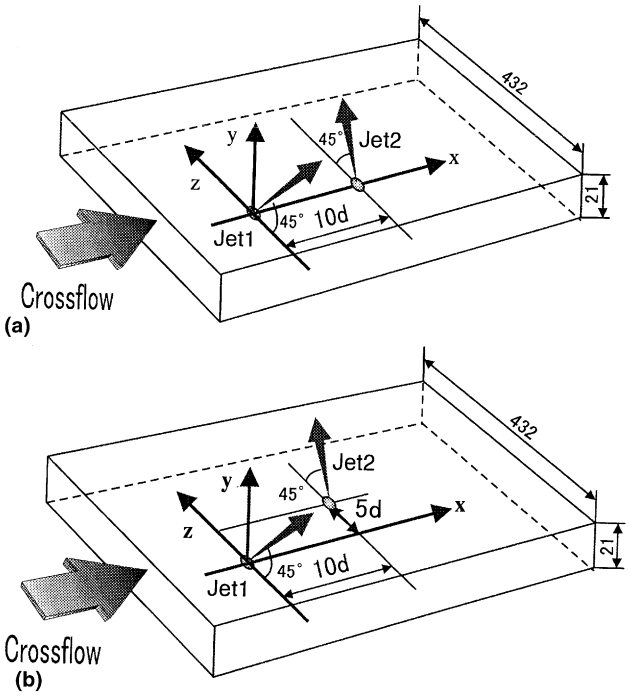

Fig. 1. Test section and twin jet nozzles. (a) In-line arrangement. (b) Staggered arrangement.

The staggered arrangement of the twin jets described in Fig. 1(b) has the same pitch angle, skew angel and separation distance as the in-line arrangement case. Only one different condition was that the downstream jet, Jet 2, was shifted spanwisely by the length of 5 nozzle-diameters. The origin of the coordinate system is located at the center of the open end of Jet 1. x-, y- and z-axes designate the streamwise, normal and spanwise directions, respectively.

The experimental set-up of flow visualization is illustrated in Fig. 2. The patterns of the jet flow field were visualized with the addition of fluorescent dye, Uranine, illuminated by a planar CW Ar^+ laser light. The cross-sectional images of the flow patterns were taken through the acrylic plate with a CCD camera set up far downstream. Velocity vectors in the cross-sections of the test section were estimated with the PIV system from the scattering images of fine TiO_2 particles injected into the jet flows and illuminated by a planer Nd:YAG pulse laser.

The temperature distributions of the heat transfer target surface were measured with thermochromic liquid crystal sheets attached to the back of the target surface. The images of the liquid crystal were taken with another different CCD camera installed above through the transparent upper wall. The colors of the images were transformed accurately and effectively into the temperatures by means of neural network technique to obtain Nusselt number distributions on the target surface (Nakabe et al., 1998b).

3. Results and discussion

3.1. In-line arrangement

Fig. 3 shows the visualization results of longitudinal vortices generated by the twin inclined impinging jets with the in-line arrangement at five streamwise locations, (a) $x/d = 5$, (b) $x/d = 10$, (c) $x/d = 20$, (d) $x/d = 30$ and (e) $x/d = 40$. The crossflow Reynolds number based on the hydraulic diameter of the test section, Re, was fixed to be constant equal to 5000, and the velocity ratio, VR, 5. White arrows drawn at $z/d = 0$ in Fig. 3(f) represent the spanwise location of the twin jets. The downstream-side jet, Jet 2, itself discharged in upper right direction was visualized at $x/d = 10$, shown in Fig. 3(b). The visualized cross-sectional images, in particular Fig. 3(c) and (d), clearly reveal that three major longitudinal vortices V1, V3 and V4, and not two pairs of counter-rotating vortices which could be expected in the previous single jet experiment (Nakabe et al., 1998a), were generated downstream of the twin jets. The schematic illustration of those three vortices is shown in Fig. 3(f). The vortices V1 and V3 with anti-clockwise rotation and the vortex V4 with clockwise rotation were observed in the

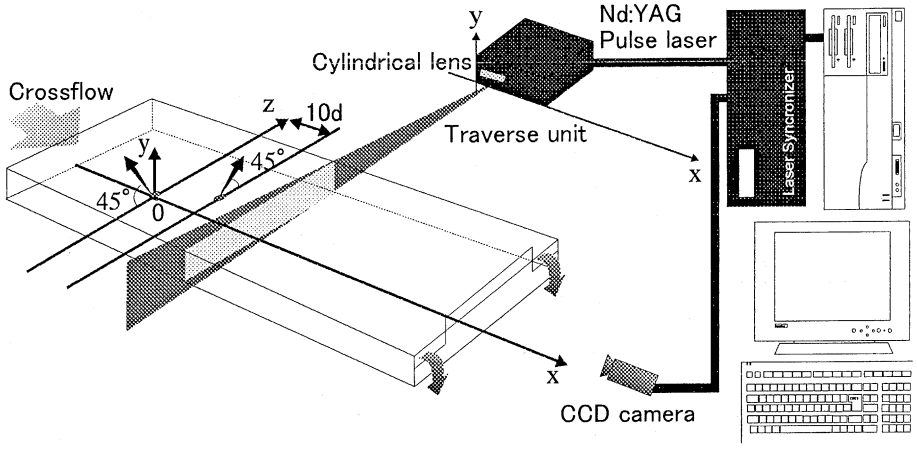

Fig. 2. Test section with flow visualization system.

cross-sectional image of the crossflow. One more small-scale clockwise-rotating vortex, V2, was faintly observed in the bottom left region next to the vortex V3. The vortices V3 and V4 form a pair of counter-rotating longitudinal vortices generated by the downstream-side jet, while V1 and V2 form a pair of vortices by the upstream-side jet. As mentioned above, the vortex V2 was obscure, small, and difficult to be recognized on a single frozen video frame. It was, however, possible to observe the motion of the vortex V2 on the screen where a time-sequential video movie was shown. The movement and strength of the vortex V3 affect the development of the vortex V2, although the discharge of each jet was done with the same intense. It was found that the interaction between the two jets has significant influence on the formation of longitudinal vortices.

The Nusselt number distributions of the in-line inclined jets for VR = 3 and 5 are shown in Fig. 4(a) and (b), respectively, under the flow condition of $Re = 5000$. The enhanced area of heat transfer was well visualized. The shape of the area could be determined by the interaction between the two inclined jets. The two regions of much higher heat transfer coefficients can be discriminated in the figures. Each of these regions includes its own maximum of Nusselt number. Two peaks of maximum Nusselt number could be observed in the regions. In the case of VR = 5, in particular, the first peak corresponding probably to the stagnation point of the upstream jet is higher than the second one formed by the downstream jet. Also, the area of higher heat transfer is much expanded in comparison with the case of VR = 3.

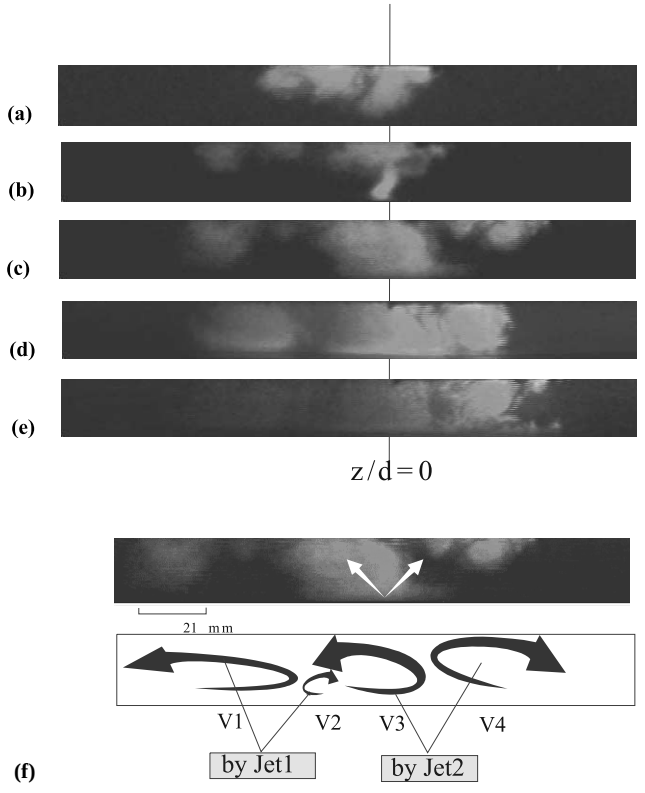

Fig. 3. Cross-sectional images of longitudinal vortices generated by twin inclined impinging jets (in-line arrangement, $Re = 5000$ and VR = 5). (a) $x/d = 5$. (b) $x/d = 10$. (c) $x/d = 20$. (d) $x/d = 30$. (e) $x/d = 40$. (f) Schematic illustration of longitudinal vortices.

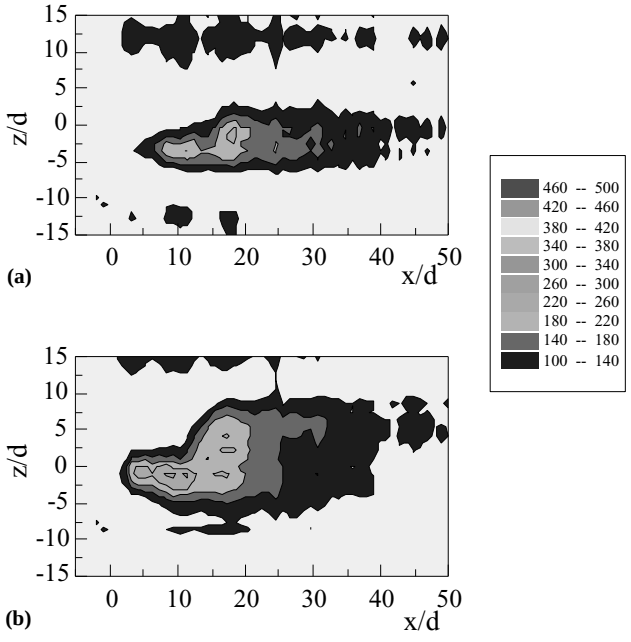

Fig. 4. Nusselt number contours (in-line arrangement, $Re = 5000$ and VR = 5). (a) VR = 3. (b) VR = 5.

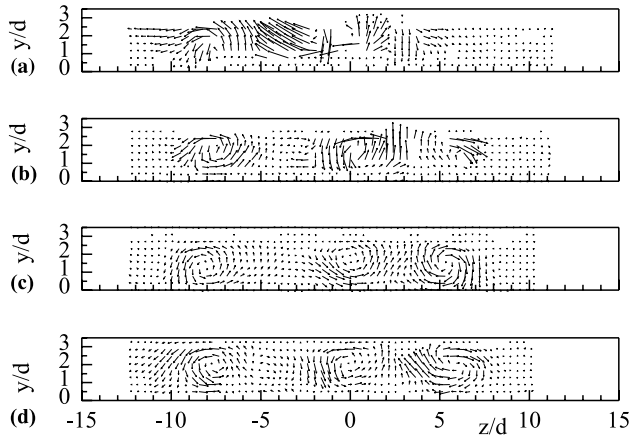

Fig. 5. Distributions of cross-sectional velocity vectors (in-line arrangement, $Re = 5000$ and VR = 5). (a) $x/d = 10$. (b) $x/d = 20$. (c) $x/d = 30$. (d) $x/d = 40$.

The velocity vector maps of the in-line arrangement are shown in Fig. 5 under the same experimental conditions, $Re = 5000$ and VR = 5, as in Figs. 3 and 4(b). The measured cross-sections were at four streamwise locations, (a) $x/d = 10$, (b) $x/d = 20$, (c) $x/d = 30$ and (d) $x/d = 40$. The three large-scale longitudinal vortices plus one small-scale vortex can be recognized in the velocity maps, corresponding to the visualized images shown in Fig. 3. These vortices were observed even far downstream from the locations of the nozzles. It can be seen that the vortices forming each of the pairs are rotating in opposite directions, and that the areas of high spanwise velocity, close to the upper target wall, are related to the region of enhanced heat transfer. Since the vortex V2 drawn in Fig. 3 was generated upstream of Jet 2, it could play an important role in modifying the growth of the vortex V3 and in shifting its location close to the target wall.

The streamwise velocity components in the near-wall regions influenced by the vortices V1 and V4 were also considerably larger. The velocity vector components orthographically projected on x–z cross-sectional plane at $y/d = 3.17$ are shown in Fig. 6. The flow in these regions sweeps over the target wall and eventually expands the heat transfer enhancement region. The comparison between the results of velocity and Nusselt number measurements reveals that very good agreement between the vortex location and heat transfer enhancement region could be obtained. The contours of the enhanced region are related to the paths of the large-scale longitudinal vortices.

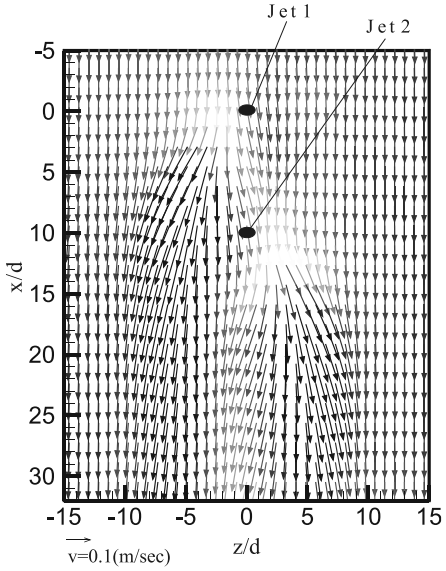

Fig. 6. Distributions of velocity vectors in the near-wall region parallel to target wall (in-line arrangement, $Re = 5000$ VR = 5 and $y/d = 3.17$).

3.2. Staggered arrangement

In Fig. 7, the results of flow visualization are presented in the case of the staggered arrangement of twin inclined jets at five streamwise locations, (a) $x/d = 5$, (b) $x/d = 10$, (c) $x/d = 20$, (d) $x/d = 30$ and (e) $x/d = 40$. The experiment was set up in the same conditions as the in-line arrangement case. It is shown in Fig. 7(f) that the cross-sectional flow patterns include four vortices marked as V1, V2, V3, and V4, respectively, from the left-hand side to the right-hand side of the illustration. These longitudinal vortices form two pairs of counter-rotating vortices, which is different from the case of in-line arrangement. The vortices V1 and V2 creating the left-hand side pair were generated by the upstream jet, Jet 1, while the vortices V3 and V4 creating the right-hand side pair were generated by the downstream one, Jet 2. The pairs grow up along the streamwise direction, but even far downstream away from the locations of the nozzles the four vortices were still observed. Thus, it can be said that the interaction between the twin inclined jets with the staggered arrangement is weaker than the one with the in-line arrangement. The spanwise distance between the jet nozzles, $5d$, in the staggered arrangement could be one of the main reasons of this difference in the present experimental set-up.

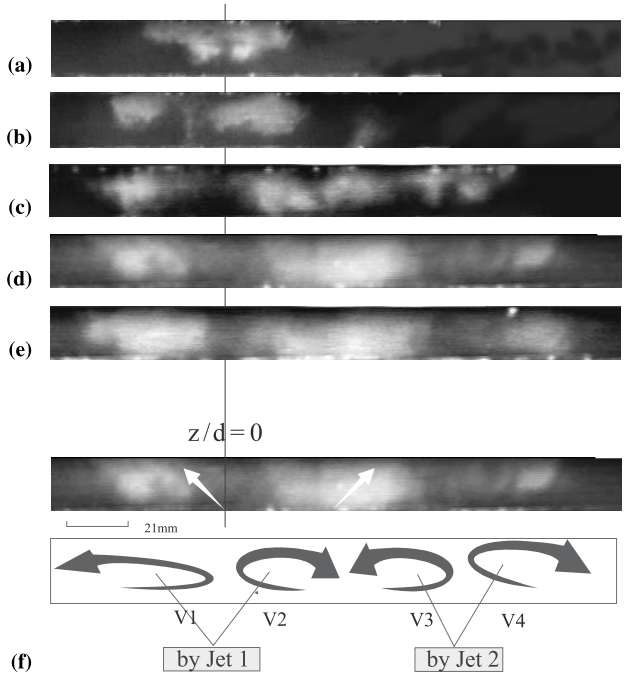

Fig. 7. Cross-sectional images of longitudinal vortices generated by twin inclined impinging jets (staggered arrangement, $Re = 5000$ and VR = 5). (a) $x/d = 5$. (b) $x/d = 10$. (c) $x/d = 20$. (d) $x/d = 30$. (e) $x/d = 40$. (f) Schematic illustration of longitudinal vortices.

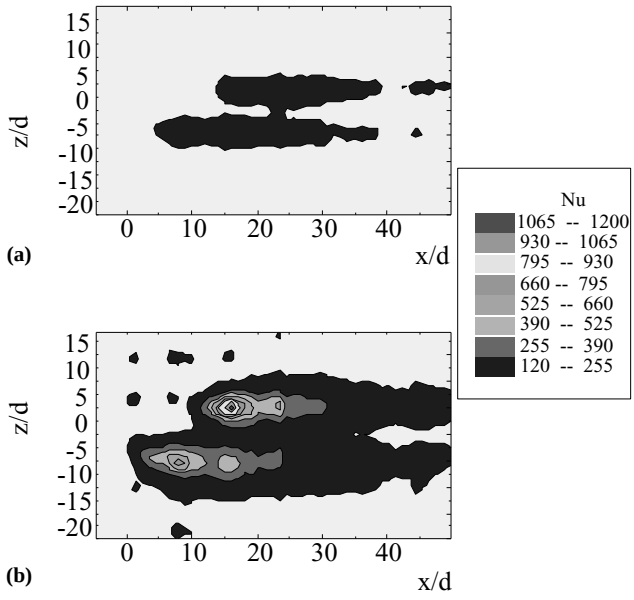

Fig. 8. Nusselt number contours (Staggered arrangement, $Re = 5000$ and VR = 5). (a) VR = 3. (b) VR = 5.

Nusselt number distributions in the staggered arrangement under the same flow conditions as the in-line arrangement are shown in Fig. 8(a) and (b). The Nusselt number distribution strongly depends on the velocity ratio, VR. The two comet-like patterns can be recognized in the Nusselt number distributions, different from the patterns in the case of the in-line arrangement. The two regions with characteristic maximum Nusselt numbers were found in both of the distributions, (a) and (b), similar to the in-line arrangement. For the case of VR = 3 shown in Fig. 8(a), it is difficult to estimate which peak is higher. The situation seems to be a little different in Fig. 8(b), where the second, downstream-side, peak corresponding to the downstream-side jet, Jet 2, is higher than the first, upstream-side, peak. In the case of the in-line arrangement, the situation was opposite, shown in Fig. 4(b), where the upstream-side peak of Nusselt number is higher than the downstream-side one.

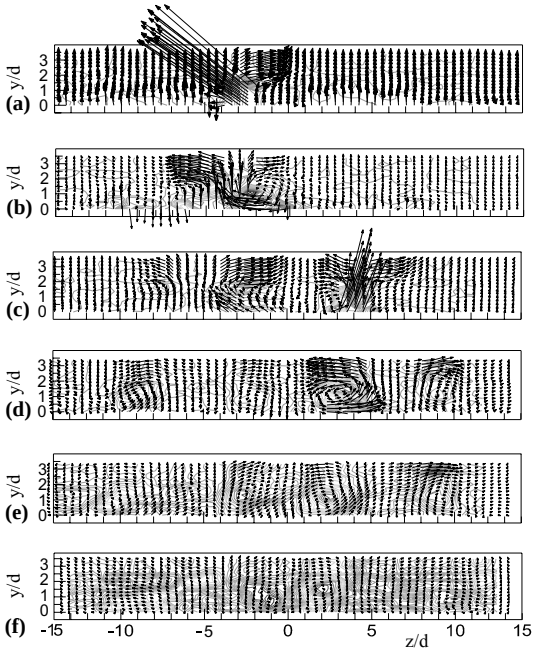

Fig. 9. Distributions of cross-sectional velocity vectors with vorticity contours (staggered arrangement, $Re = 5000$ and VR = 5). (a) $x/d = 0$. (b) $x/d = 5$. (c) $x/d = 10$. (d) $x/d = 20$. (e) $x/d = 30$. (f) $x/d = 40$.

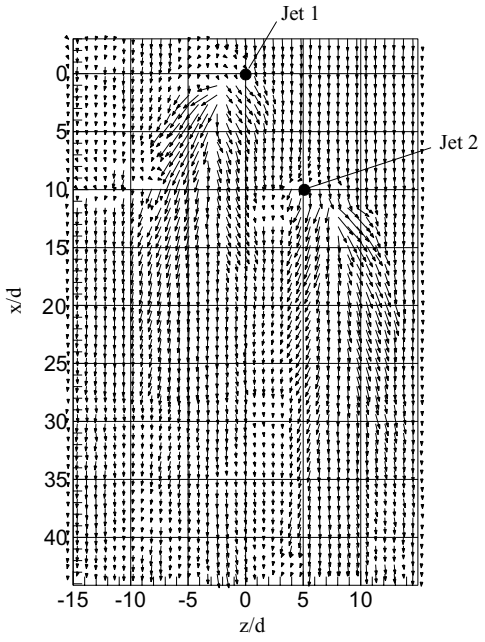

Fig. 10. Distributions of velocity vectors in the neasr-wall region parallel to target wall (staggered arrangement, $Re = 5000$, VR = 5 and $y/d = 3.17$).

Fig. 9 shows the vector maps of the velocity components in the cross-sections normal to the crossflow direction in the staggered arrangement under the same flow conditions as the above case, $Re = 5000$ and VR = 5. The vorticity contours are also shown in the same figure, which corresponds well to the visualized images of the vortices shown in Fig. 7. Fig. 10 shows the vector maps of vector components orthographically projected on x–z cross-sectional plane at $y/d = 3.17$, in the near-wall region under the same conditions. The locations of the longitudinal vortices in the staggered arrangement case correspond very well to the enhanced region of heat transfer, similar to the in-line arrangement case. It was found in the velocity vector maps at the streamwise locations, (a) $x/d = 0$ and (c) $x/d = 10$, in Fig. 9 that the impingement angle of the downstream-side jet is closer to 90° than the one of the upstream-side jet. This could be a reason why the downstream peak is larger than the upstream one in the staggered arrangement. The top view of the velocity vectors shown in Fig. 10 shows that the upstream impinging flow spreads spanwisely wider than the downstream one, corresponding to the above-shown Nusselt number distributions.

4. Conclusions

The flow visualization, heat transfer measurements and velocity measurements were made for twin inclined jets in in-line and staggered arrangements with crossflow. The experimental results obtained in the present study are summarized as follows:

1. The large-scale longitudinal vortices are generated in the rectangular duct flow as the result of inclined impinging jets. The number of vortices depends on the arrangement of the jet nozzles. For the in-line arrangement, three large-scale vortices are observed, while for the staggered arrangements, four ones are found.
2. The path of the longitudinal vortices corresponds very well to the heat transfer enhancement regions for both kinds of jet nozzles' arrangement. The upstream peak of Nusselt number value is higher than the downstream one in the case of in-line arrangement. The opposite trend can be observed in the case of the staggered arrangements; the downstream peak is higher than the upstream one.
3. The interaction between the jets depending on the nozzles' arrangements has serious influence on the vortical structure and also on the enhanced heat transfer regions.

Acknowledgements

Partial support from the Grant-in-Aids of Scientific Research, Ministry of Education, Science and Culture, Japan for the present experimental research is greatly appreciated.

References

Bouchez, J.P., Goldstein, R.J., 1975. Impingement cooling from a circular jet in a cross flow. Int. J. Heat Mass Transfer 18, 719–730.

Fornalik, E., Nakabe, K., Yamamoto, Y., Chen, W., Suzuki, K., 1999. Visualization of heat transfer enhancement regions modified by the interaction of inclined impinging jets into crossflow. Machine Graphics Vision 8, 597–610.

Goldstein, R.J., Behbahani, A.I., 1982. Impingement of a circular jet with and without cross flow. Int. J. Heat Mass Transfer 25, 1377–1382.

Huang, Y., Ekkad, S.V., Han, J.C., 1996. Detailed heat transfer coefficient distributions under an array of inclined impinging jets using a transient liquid crystal technique. In: Ninth International Symposium on Transport Phenomena II, pp. 807–812.

Metzger, D.E., Korstad, R.J., 1972. Effects of crossflow on impingement heat transfer. Trans. ASME; J. Eng. Power 94, 35–42.

Nakabe, K., Suzuki, K., Inaoka, K., Higashio, A., Acton, J.S., Chen, W., 1998a. Generation of longitudinal vortices in internal flows with an inclined impinging jet and enhancement of target plate heat transfer. Int. J. Heat Fluid Flow 19, 573–581.

Nakabe, K., Higashio, A., Chen, W., Suzuki, K., Kim, J.H., 1998b. An experimental study on the flow and heat transfer characteristics of longitudinal vortices induced by an inclined impinging jet into a crossflow. In: 11th International Heat Transfer Conference, vol. 5, pp. 439–444.

Nakabe, K., Yamamoto, Y., Fornalik, E., Chen, W., Suzuki, K. 1998c. Visualizations of obliquely discharged jet flows and their heat transfer enhancement regions. In: CD-Rom of Eighth International Symposium on Flow Visualization, Torrento, Italy, ISBN 09533991 0 9.

Saad, N.R., Mujumdar, A.S., Messeh, W.A., Douglas, W.J.M., 1980. Local heat transfer characteristics for staggered arrays of circular impinging jets with cross-flow of spent air. ASME paper 80-TH-23, 105–112.

Son, J.W., Kwan, G.H., Sohn, J.L. 1996. Measurement of heat transfer coefficients inside turbine cooling blades in gas turbine engine using thermal imaging technique. In: Third KSME/JSME Thermal Engineering Conference, Kyongju, Korea, pp. III-89– III-92.

Sparrow, E.M., et al., 1975. Effect of nozzle – surface separation distance on impingement heat transfer for a jet in a crossflow. Trans. ASME; J. Heat Transfer 97, 528–533.